Reaction Chemistry & Engineering

Intermediate Temperature Water-Gas Shift Kinetics for Hydrogen Production

Journal:	*Reaction Chemistry & Engineering*
Manuscript ID	RE-ART-03-2019-000121.R1
Article Type:	Paper
Date Submitted by the Author:	29-May-2019
Complete List of Authors:	Houston, Ross; University of Tennessee, Biosystems Engineering and Soil Science Labbe, Nicole; The University of Tennessee, Center for Renewable Carbon Hayes, Douglas; University of Tennessee Knoxville, Biosystems Engineering and Soil Science; Oak Ridge National Laboratory, Daw, Charles; University of Tennessee, Biosystems Engineering and Soil Science; Oak Ridge National Laboratory, Abdoulmoumine, Nourredine; University of Tennessee, Biosystems Engineering and Soil Science; University pf Tennessee

Journal Name

ARTICLE

Intermediate Temperature Water-Gas Shift Kinetics for Hydrogen Production

eReceived 00th January 20xx,
Accepted 00th January 20xx

DOI: 10.1039/x0xx00000x

www.rsc.org/

Ross Houston,[a] Nicole Labbé,[b] Douglas Hayes,[a] Charles Daw,[c,d] and Nourredine Abdoulmoumine*[a,b]

The water-gas shift (WGS) reaction is an attractive process for producing hydrogen gas from lignocellulosic biomass conversion applications. The goal of this study was to investigate hydrogen production via the WGS reaction using carbon monoxide (CO), one of the significant non-condensable gases formed during biomass fast pyrolysis, as reactant over the range of the intermediate-temperature shift (ITS). WGS reaction is typically carried out as a low-temperature shift (LTS;150-300 °C) or a high-temperature shift (HTS; 300-500 °C) with each shift using a different catalyst. In this study, the WGS was conducted at an intermediate temperature range (200-400 °C) relevant to lignocellulosic biomass fast pyrolysis hydrodeoxygenation over a copper (Cu) based catalyst in a CO-lean environment (70 vol. % steam, 20 vol. % He, and 10 vol. % CO). The experimental temperatures were tested over three different weight hourly space velocities (WHSV =1220, 2040, and 6110 cm^3/g-min). CO conversion increased with increasing temperature and catalyst weight, with a maximum CO conversion of 94% achieved for temperatures greater than 300 °C. We evaluated four models including two mechanistic Langmuir-Hinshelwood (LH) models, one redox mechanistic model, and one reduced order model (ROM). The first (LH1) and second (LH2) Langmuir-Hinshelwood models differ by the intermediate formed on the catalyst surface. LH1 forms product complexes while LH2 produces a formate complex intermediate. LH2 best described our experimental kinetic data, based on statistical and regression analysis, and provided apparent activation energies between 60 and 80 kJ/mol at different space velocities. Furthermore, the ROM fit the experimental data well and, due to its simplicity, has potential for incorporation into computationally expensive simulations for similar experimental conditions.

Introduction

The water–gas shift reaction (WGS) has been an important reaction in chemical industrial processes for decades, especially in the production of hydrogen gas[1]. Today, concerns over the environmental impact of fossil fuels and the increasing energy demand have encouraged the development of cleaner and sustainable energy sources, which makes the production of hydrogen (H_2) even more relevant. Hydrogen can be either directly used as an energy source or as an upgrading agent to produce high-quality biofuels[2, 3]. In the WGS reaction, as shown below, carbon monoxide (CO) reacts with steam (H_2O) in the presence of a catalyst to produce carbon dioxide (CO_2) and hydrogen (H_2), the highest energy carrier of renewable energy intermediates[4].

$$CO + H_2O \leftrightarrow H_2 + CO_2$$

For industrial processes using a reactant stream with high CO concentration, e.g.,>50 vol. %[5], the WGS reaction is usually separated into two stages for increased conversion: high-temperature shift (HTS) and low-temperature shift (LTS)[6], characterized by specific reaction temperatures as well as catalyst types. HTS takes place above 300 °C and commonly uses iron/chromium oxide catalysts[7, 8], while LTS occurs in the range of 150 to 300 °C and typically utilizes a copper-based catalyst[9].

The kinetics of HTS and LTS have been well studied given the industrial significance of these processes. Indeed, previous mechanistic studies have shown that Langmuir-Hinshelwood kinetics best fitted experimental LTS data over a copper-based catalysts[10-12]. Conversely, there is no clear consensus as to which mechanism best describes the HTS[13, 14]. The HTS has generally been seen to proceed via a reduction-oxidation mechanism over iron-based catalysts[15-17]. However, other studies have found HTS data best fit with

[a] Department of Biosystems Engineering and Soil Science, University of Tennessee, 2506 E.J. Chapman Dr, Knoxville, TN 37996, USA.
[b] Center for Renewable Carbon, University of Tennessee, 2506 Jacob Drive, Knoxville, TN 37996-4542, USA.
[c] Department of Mechanical, Aerospace and Biomedical Engineering, University of Tennessee, Knoxville, TN 37996, USA.
[d] National Transportation Research Center, Oak Ridge National Laboratory, Oak Ridge, TN 37932, USA.

Langmuir-Hinshelwood and empirical power law models[10, 18, 19].

While the HTS and LTS staging is feasible in applications solely focused on producing H_2, a two-stage WGS system is not always practical for applications that occur at temperatures at the edge of both the LTS and HTS ranges. This is the case, for example, in the hydrodeoxygenation of bio-oil produced from biomass pyrolysis. Hydrodeoxygenation occurs at intermediate temperature shift (ITS) between 200 and 400°C[20, 21]. Yet, there is limited research on WGS kinetics available at ITS conditions that cover both LTS and HTS domains. Furthermore, while multiple rate law models have been used to derive the kinetics of WGS[10], no clear consensus has yet emerged[22, 23]. The lack of an agreed upon kinetic model for WGS, especially for ITS, makes advanced modeling of these processes almost impossible. These gaps justify the present study which aims to identify the appropriate rate law and to derive the WGS kinetics at intermediate temperatures (200-400 °C).

Experimental

Catalyst preparation and characterization

A commercial copper-based, low-temperature WGS catalyst (HiFUEL® W220) was obtained from Alfa Aesar (Haverhill, MA, USA) and used for this study. This catalyst was chosen to investigate the ITS because copper-based catalyst has reached a consensus for the WGS mechanism in LTS than iron-based catalysts. Therefore, the copper-based catalyst provided a good starting point for potential mechanisms. The catalyst was first size reduced by a mortar and pestle and sieved to particle sizes between 0.425 and 0.595 mm (30-40 mesh). The catalyst was then characterized by physisorption for surface area and pore volume. A Beckman Coulter surface area analyzer was used to determine the catalyst's Brunauer-Emmett-Teller (BET) surface area and total pore volume using N_2 as an adsorbate. The catalyst samples were outgassed for 60 min at 120 °C[24]. Additionally, the catalyst was tested for the optimal reduction temperature using temperature program reduction (TPR) by a thermogravimetric analyzer (TGA) (Perkin Elmer, Pyris 1, Waltham, MA, USA)[25-27]. Approximately 30 mg of catalyst were placed on the sample pan to undergo TPR. The sample was then outgassed by heating to 105 °C at 25 °C/min, under a flow of helium, and maintained for 45 min to remove any adsorbate present in and on the catalyst. The outgassed sample was then heated from 105 to 400 °C at a rate of 2 °C/min under a constant reducing gas (90% N_2, 10% H_2) flow. Upon completion, the sample's differential thermogravimetric curve was generated, using fityk software[28], and the peak minima, indicative of the maximum mass loss, was taken at the reduction temperature. All experiments were conducted in triplicate.

Kinetic measurements

WGS experiments were carried in a plug flow reactor (PFR) system outfitted with a feed water delivery and steam generation system, as illustrated in Figure 1. The system consists of He and CO supply lines, each equipped with a mass flow controller, a syringe pump for delivering water (Chemyx Inc., 10060, Stafford, TX, USA), an evaporator for generating steam, a ½ inch (12.7 mm) tube plug flow reactor (PFR) housed in a split tubular furnace (Applied Test Systems, 3210, PA, USA), a set of condensers in series, and gas scrubbing tubes with activated carbon and drierite (W.A. Hammond Drierite Co., Xenia, OH, USA). The catalytic experiments were carried out at reactor temperatures of 200 to 400 °C in 50 °C temperature intervals. The temperature of the bed was monitored by a K-type thermocouple, which fed back to a proportional integral derivative (PID) controller that controls the furnace. In addition to the temperature, the space velocity (SV), reported as weight hourly space velocity (WHSV, $cm^3/(min\text{-}g)$), varied from 6110 (WHSV #1), 2040(WHSV #2), and 1220(WHSV #3). These WHSVs were calculated using the run conditions for 200 °C at 0.1 g, 0.3 g, and 0.5 g of active catalyst, respectively. An increase in the active catalyst weight at a given temperature reduces the WHSV. The reactor bed consisted of the copper-based catalyst diluted with alumina (γ-Al_2O_3), of the same particle size, for catalyst quantities under 0.5 g to provide the desired space velocity and avoid channeling in the reactor. Before every experiment, the catalyst is reduced *in-situ* using a gas mixture containing 10 vol. % H_2 and 90% N_2 for two hours at the appropriate reduction temperature. Afterward, the CO and carrier gas (He) streams were controlled by two mass flow controllers before combining with a stream of water pumped into the evaporator by the syringe pump. The evaporator served to convert the water to steam as well as preheat the gases before reaching the reactor. Upon entering the reactor, CO and steam underwent the WGS reaction. The product gases were sent to a condenser to remove any excess steam from the product stream. WGS experiments were carried out in a CO-lean environment (70 vol. % water, 20 vol. % He, and 10 vol. % CO) with a steam to carbon monoxide ratio (S/C) ranging from 5 to 7, thereby favoring higher CO conversion due to CO serving as the limiting reactant.

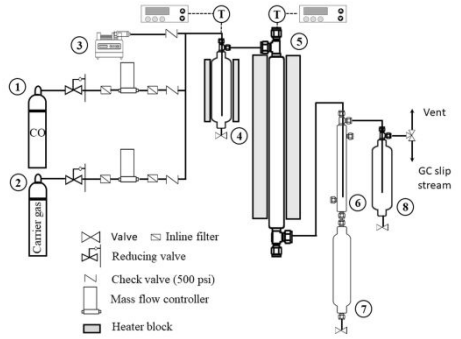

Figure 1. Experimental catalytic reactor setup. 1. Carbon monoxide delivery lines; 2. Inert gas (He) delivery line; 3. High-pressure syringe water pump; 4. Onboard steam generator with PID controlled heaters; 5. Packed bed reactor with PID controller furnace heater; 6. Shell and tube heat exchanger; 7. Liquid collection reservoir with bottom drain valve; 8. Overflow reservoir with a bottom drain valve.

At the PFR outlet, a slipstream of the effluent gas was continuously delivered to a 6 port actuating valve with a 1 ml sampling loop connected to a SRI TCD/FID/FPD gas chromatograph (GC) equipped with a thermal conductivity detector (TCD) (SRI Instruments Inc., 8610C CA, USA) where the gas composition was analyzed continuously while the remainder of the outlet stream was vented to the fume hood. Helium served as the eluent for a two-column series system. The first column, a 6' molecular sieve 13x column, analyzes a majority of the products, mainly H_2 and CO, while the second column, 6' Hayesep-N column, is used to detect the CO_2. The temperature program was set with an initial temperature of 40 °C and is held for 10 minutes before ramping to 80 °C with a rate of 20 °C/min. The peak of interest was the CO peak. Before each experiment, the GC was calibrated for peak area vs. concentration by using a calibration gas cylinder with the following concentrations: 5 vol. % CO, 5 vol. % CO_2, 5 vol. % N_2, 4 vol. % oxygen (O_2), 4 vol. % methane (CH_4), 4 vol. % H_2, and balance helium. The GC sampling loop was flushed with the calibration gas, and the analysis was repeated at least three times. At the beginning of each experiment, streams of CO and He were sent to the GC to determine the initial amount of the CO entering the reactor. The product stream was analyzed in the GC, and the amount of CO and conversion at the outlet was determined for each experimental condition.

Kinetic analysis and modeling

Kinetic data analysis

Using well-documented WGS reaction mechanisms and data obtained from the laboratory scale experiments, kinetic parameters, such as the reaction order, rate constant, and activation energy, were derived[29]. Preliminary screening was carried out to test for external mass transfer and diffusion limitations for the proposed operating conditions. The mass transfer coefficient is inversely proportional to the boundary layer thickness. At lower velocities, the boundary layer is thick, and the mass transfer rate limits the overall reaction rate while at higher velocities, reactants and products rapidly diffuse across the boundary layer quickly and mass transfer no longer limits the reaction[29]. If there are external mass transfer limitations, the higher gas velocities will lead to a higher conversion of CO.

External mass transfer limitations were assessed using the Carberry number (Ca)[30]. Ca is a ratio of the observed reaction rate to the maximum external mass transfer rate, shown below

$$Ca = \frac{\left(-r_{CO}^{obs}\right)\rho_c}{a' k_f C_{CO}^b} < 0.05$$

where $-r_{CO}^{obs}$ is the observed reaction rate, ρ_c is the density of the catalyst particle, a' is the specific external surface area of the catalyst particle, k_f is the mass transfer coefficient, and C_{CO}^b is the CO concentration in the bulk phase[31]. The observed reaction rate was calculated via the postulated reaction rate in Matlab and further confirmed by calculating the area under the curve of a plot of W/F_{co} vs conversion where W is weight of active catalyst and F_{co} is the molar flow rate of CO. Furthermore, internal diffusion limitations tests were carried out using the Weisz-Prater criterion.

$$\frac{\left(-r_{CO}^{obs}\rho_c R_p^2\right)}{\left(D_e C_{As}\right)} \ll 1$$

where R_p is the mean radius of the catalyst particle (m), D_e is the effective diffusivity of CO in the catalyst (m^2/s), and C_{As} is the CO concentration on the catalyst surface. The effective diffusivity is calculated value using properties of the catalyst

$$D_e = \frac{\mathrm{D}\varphi_p\sigma}{\tau}$$

where D is the diffusion coefficient of CO in steam, φ_p is the porosity of the catalyst particle (product of the pore volume and the effective particle density having a typical value of 0.4 for a catalyst pellet). σ is the constriction factor with a typical value of 0.8, and τ is the tortuosity with a typical value of 3.0[32, 33]. If the criteria are satisfied, there is no external or internal diffusion limitation.

Thermodynamic analysis

The WGS reaction is a reversible, exothermic reaction and thermal equilibrium is more rapidly achieved at higher temperatures[8]. Due to the exothermic nature of the reaction, the equilibrium constant as well as the carbon monoxide tend to decrease as temperature increases[15].

$$K_{eq} = \frac{[H_2]_{eq}[CO_2]_{eq}}{[CO]_{eq}[H_2O]_{eq}}$$

The equilibrium conversion of CO depends on the molar ratio of steam to CO supplied to the system, S/C (>1). Therefore, the equilibrium constant can be rewritten

$$K_{eq} = \frac{X^2}{(1-X)(\frac{S}{C}-X)}$$

where X is the equilibrium conversion of CO, the limiting reactant. The theoretical equilibrium constant was calculated using the Gibbs energy of reaction (ΔG_{rxn}), which was then used to calculate the theoretical equilibrium conversion.

$$K_{eq} = \exp\left(\frac{-\Delta G_{rxn}}{RT}\right)$$

Kinetic models

Multiple kinetic models have been explored to determine the reaction kinetics and rate of reaction for the WGS reaction[10]. The mechanism of the WGS is primarily believed to proceed via one of two pathways: an associative mechanism or a redox mechanism. The associative mechanism is accepted as prevalent for LTS; however, the prevalent mechanism for HTS is still up for debate[13, 34]. In the case of ITS, there are no proposed mechanisms specifically for the temperature range between LTS and HTS. Therefore, the kinetic mechanisms investigated were the ones that have shown to fit either the LTS or HTS. Three mechanistic models and one empirical model were proposed to fit the experimental results. In all models, the Arrhenius equation was used to model the temperature dependence of rate constant, *k*,

$$k = A_0 e^{\frac{-E_A}{RT}}$$

where A_0 is the pre-exponential factor, E_A is the activation energy, *R* is the gas constant and *T* is temperature.

Langmuir-Hinshelwood mechanism and model

Armstrong and Hilditch proposed a model based on the associative form of the Langmuir-Hinshelwood (LH) mechanism in 1920[35] where CO and H_2O undergo adsorption onto the catalyst surface to produce intermediates that desorb from the catalyst into the products of CO_2 and H_2[36]. Researchers have tried to prove the exact form of the intermediates on the catalyst surface, such as formates[15, 37]. Ayastuy et al. performed an extensive test that included eight possible LH mechanisms with different active sites and intermediate formation steps to investigate WGS kinetics of the LTS and two associative mechanisms were shown to give the best fit[11]. Each LH mechanism was derived through the proposed elementary reactions of the WGS. These associative mechanisms were further investigated by Mendes et al. and found agreeable results[12]. Our catalyst is similar to the one used by previous authors, therefore we investigated these mechanisms in our study. The first LH mechanism (LH1) is described by the following general reactions, where S represents a vacant adsorbing site on the catalyst and S·, for example CO·S, is indicative of an adsorbed species, in this case, CO (note: the S· bonds are not true covalent bonds. Therefore, the octet rule is not violated)[11, 36].

$$CO + S \leftrightarrow CO \cdot S$$
$$H_2O + S \leftrightarrow H_2O \cdot S$$
$$CO \cdot S + H_2O \cdot S \leftrightarrow CO_2 \cdot S + H_2 \cdot S$$
$$H_2 \cdot S \leftrightarrow H_2 + S$$
$$CO_2 \cdot S \leftrightarrow CO_2 + S$$

For the LH1, the rate-limiting step (RLS) is the surface reaction between adsorbed species. The second LH mechanism (LH2) undergoes the same initial reactions of CO and H_2O adsorbing onto an active site. The differences between the two mechanisms occur from the adsorbed species reacting to form an absorbed intermediate species instead of adsorbed product species. The adsorbed intermediates then react to produce CO_2 and H_2.

$$CO + S \leftrightarrow CO \cdot S$$
$$H_2O + S \leftrightarrow H_2O \cdot S$$
$$CO \cdot S + H_2O \cdot S \leftrightarrow COOH \cdot S + H \cdot S$$
$$COOH \cdot S \leftrightarrow CO_2 + H \cdot S$$
$$2H \cdot S \leftrightarrow H_2 + 2S$$

The RLS for the second mechanism is also the surface reaction between the two adsorbed reactant species; however, this time to produce a formate intermediate and adsorbed hydrogen.

Redox mechanism and model

In 1949, Kulkova and Temkin hypothesized that the WGS proceeded through a series of reduction and oxidation reactions where water disassociated onto the catalyst surface to produce hydrogen, and then CO reduced the catalyst surface to produce CO_2 according to the mechanism below.

$$H_2O + S \leftrightarrow H_2 + O \cdot S$$
$$CO + O \cdot S \leftrightarrow CO_2 + S$$

where * represents a vacant active site analogous to the one introduced earlier in the associate mechanism[38]. The RLS for the proposed reduction mechanism consists of water adsorbing on an active site and releasing hydrogen while oxidizing the vacant site[12]. The regenerative, or reduction, mechanism provides a better fit to the HTS experiments rather than to the LTS[39]. While the LH mechanisms have a consensus for being the most representative mechanism for the LTS, the predominant

mechanism is still up for debate. The HTS is typically thought to proceed through either a redox mechanism or an LH mechanism[19, 40].

Reduced order model

In addition to the mechanistic models, the experimental data were fit to a reduced order model (ROM) to facilitate incorporating the WGS kinetics into computationally expensive process models, e.g., vapor phase upgrading, where simpler ROM models can significantly reduce computational resources. Unlike mechanistic models, ROMs are not dependent on specific reaction mechanism and are limited to specific operating conditions[23, 36]. Consequently, the resultant rate expression is empirical and provides a simpler expression that is computationally lighter than the mechanistic expressions[41]. The rate expression for the empirical power law is represented by

$$-r_{CO} = kP_{CO}^{a}P_{H_2O}^{b}P_{H_2}^{c}P_{CO_2}^{d}(\beta)$$

where a, b, c, and d are the reaction orders for CO, H_2O, H_2, and CO_2, respectively. P_i is the partial pressure of each species. The WGS reaction is reversible, therefore the backwards reaction must be accounted for. The β term simulates the reaction's approach to chemical equilibrium and is described below.

$$\beta = 1 - \frac{P_{H_2}P_{CO_2}}{P_{CO}P_{H_2O}K_{eq}}\ 1$$

Parameter estimation and model discrimination

A numerical optimization method was adopted for estimating the parameters of both the mechanistic models and the ROM. A Matlab code was developed that utilizes an ordinary differential equation (ODE) subroutine and non-linear regression analysis, using the non-linear least squares solver function (*lsqcurvefit*), which has been used previously for kinetic studies[42]. Initial guesses for parameters were taken from existing kinetic studies on WGS[11, 12, 36] and multiple statistical tests, such as the root mean squared error (RMSE), mean absolute error (MAE), a goodness of fit (FIT), and the Akaike Information Criterion (AIC) were applied for each data set.

$$RMSE = \sqrt{\frac{1}{N}\sum_{i=1}^{N}(y_i - F(k,x_i))^2}$$

$$MAE = \frac{1}{N}\sum_{i=1}^{N}|y_i - F(k,x_i)|$$

$$FIT = 100\frac{\sum_{i=1}^{N}\frac{(y_i - F(k,x_i))^2}{N^2}}{experimental_{max}}$$

$$AIC = N * log\left(\frac{\sum(y_i - F(k,x_i))^2}{N}\right) + 2k$$

where $F(k,x_i)$ are the values calculated by the model, k is the number of parameters being optimized, N is the number of observations, and y_i is the experiental data, and $experimental_{max}$ is the maximum observed value[43, 44]. Since kinetic data are only collected every 13 minutes, a piecewise cubic Hermite interpolating polynomial (PCHIP) function[45] was used to generate additional interpolated points between two experimental data points. In the end, a dataset of 100 individual points was used for each parameter estimation.

Model discrimination was carried out through comparison of the results of all the statistical tests. The AIC[46] takes the number of parameters, the sample size and the residual sum of squares into account. The AIC allows for discrimination of different models with varying numbers of parameters. The model with the lowest AIC was determined to fit the data best.

Results and Discussion

Catalyst characterization

The composition of the catalyst used in this study is shown in Table 1. It is composed of copper (II) oxide, zinc oxide, aluminum oxide, and carbon in a weight percent ratio of 52:30:17:1, respectively. Cu-based catalysts have been studied extensively for low-temperature WGS reactions; however, the chemical composition of the oxide components can differ greatly, from 8 wt. % CuO[47] to 50 wt. % CuO[12]. Previous studies have used similar catalysts containing $CuO/ZnO/Al_2O_3$[11, 12, 15, 23, 47, 48] and others impregnated copper onto a supported metal oxide with a maximum loading of 20 wt. %[9, 49, 50]. This study utilizes a commercial catalyst with a larger CuO content (52 wt. %) compared to most other $CuO/ZnO/Al_2O_3$ catalysts used for WGS kinetics studies[11, 12, 47, 48]. The results of the BET surface area analysis are shown in Table 2. Gines et al. studied the effect of Al_2O_3 support on catalytic activity[51]. In addition to the activity of the catalyst, the support also plays a role by increasing the overall surface area of a catalyst. Ayastuy et al. reported a BET surface area of 92 m^2/g (24.9/43.7/31.4 wt. % $CuO/ZnO/Al_2O_3$)[11] while Shen et al. used a $CuO/ZnO/Al_2O_3$ catalyst with a BET surface area of 77 m^2/g, (30.7/45.3/23.91 wt. % $CuO/ZnO/Al_2O_3$)[52]. When plotting these surface areas as well as the one used in this study as a function of Al_2O_3 content, a positive linear relationship is discovered. Therefore, the surface area is in agreement with previous reported literature values.

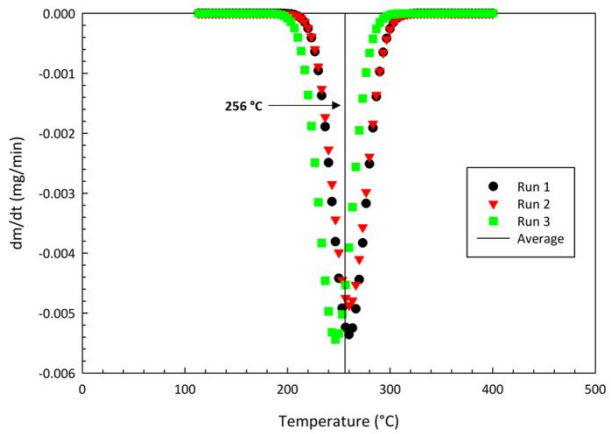

Figure 2. Results from the TPR of the commercial Cu-based catalyst showing derivate of mass as a function of temperature for each run and the average peak temperature.

Additionally, the catalyst was tested for the optimal reduction temperature using temperature program reduction (TPR). TPR produced a thermogravimetric (TG) curve mapping the mass loss of the sample as a result of the catalyst deoxygenation by hydrogen versus temperature. The TG data were then converted to a differential thermogravimetric (DTG) curve, which showed the rate of mass loss versus temperature, and fit to a curve using fityk software. A peak for the derivative of mass loss vs. temperature is indicative of reduction because the catalyst is initially oxidized. As hydrogen is transported over the catalyst at increasing temperatures, the oxygen present in the oxide is removed, resulting in a loss of mass. The TPR results are shown in Figure 2 with an optimal reduction temperature of 256 ± 8 °C. This value was similar to the catalyst supplier's recommended maximum reduction temperature of 270 °C.

Table 1. Composition of the commercial Cu-based catalyst as reported by the manufacturer.

Species	Percent (wt. %)
Copper Oxide (CuO)	52.0
Zinc Oxide (ZnO)	30.0
Aluminum Oxide (Al_2O_3)	17.0
Graphite (C)	1.0

Table 2. Catalyst characterization results.

Property	Value *
Total Pore Volume (ml/g)	0.22±0.01
BET Surface Area (m^2/g)	62.2±0.95

* ± indicates standard deviation for triplicate runs

Mass transfer and diffusion limitations

The reaction setup was tested for external mass transfer and internal diffusion limitations. External mass transfer limitations were tested for using the Carberry number (Ca)[53, 54]. The values for Ca were found to be significantly lower than 0.05; therefore, we can assume external mass transfer limitations were not present[53]. The diffusion transfer limitations were tested for using the Wheeler-Weisz criterion. This Wheeler-Weisz criterion yielded values significantly less than 0.10. Therefore, diffusion limitations were not present in the WGS experiments.

Effect of temperature and catalyst weight on carbon monoxide conversion

The bench-scale WGS reaction was carried out for five temperatures at three different WHSVs for a total of 15 experimental conditions. A comparison of CO conversion over time for WHSV #1 at each temperature is shown in Figure 3. The overall CO conversion increased and the time required to reach steady-state decreased as the temperature was increased. The latter trend reflects a limitation in the experimental design. Very few kinetic measurements in this study were collected before steady-state was reached due to limitations in the sampling frequency achievable via gas chromatography. Figure 4 displays CO conversion at steady-state as a function of temperature for each WHSV. The conversion of CO increased with both an increase of temperature and increase of catalyst weight (decreasing WHSV) until reaching a maximum conversion of 94% at 300 °C. As the temperatures were increased above 300 °C, the difference in CO conversion between the varying WHSVs decreased to a point where there was no significant difference in conversion between WHSV #2 (2040 cm^3/g-min) and WHSV #3 (1220 cm^3/g-min). WHSV #1 (6110 cm^3/g-min) produced significantly less CO than the other two. This can be attributed to the smaller amount of active catalyst present in the reactor bed. When observing the equilibrium CO conversion vs. the inverse WHSV (W/F), where W is the weight of active catalyst (g) and F is the total flow rate (cm^3/min), the maximum conversion (94%) occurred at 350 °C. This behavior is in agreement with the reported increase of CO conversion with an increase of residence time[6]. Overall, the trends observed in Figures 3 and 4 are in agreement with previous studies[11, 12, 55, 56]. Another experimental limitation that must be addressed is the length of experiments. The finite volume of steam available to be used limited run times to a few hours. Due to this shorter time on stream, there was no significant catalyst deactivation. Copper catalysts have been shown to exhibit catalyst deactivation at higher temperatures, which may be evident for longer times on stream or a full continuous process in an industrial setting. The results presented here assume no catalyst deactivation.

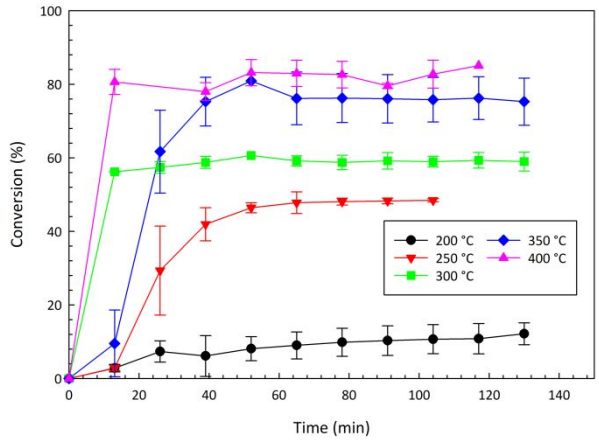

Figure 3. CO conversion as a function of time at each temperature for WHSV #1 (1220 cm³/g-min) for 200 °C, 250 °C, 300 °C, 350 °C, and 400 °C.

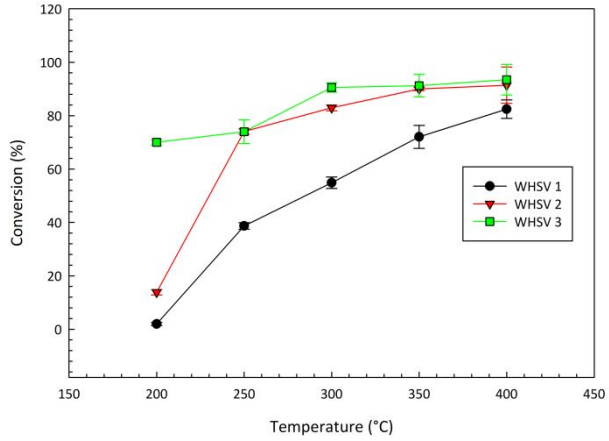

Figure 4. Steady-state CO conversion (%) as a function of temperature (°C) over different WHSVs (WHSV #1 = 1220 cm³/g-min, WHSV #2 = 2040 cm³/g-min, and WHSV #3 = 6110 cm³/g-min).

Kinetic model parameter optimization

Four possible kinetic models were evaluated through non-linear regression to obtain optimized parameters that fit best the experimental data. The rate expressions for each model are shown in Table 3. Assuming the gases behave ideally, the partial pressure of each species was calculated as follows:

$$P_{CO} = CO_0(1 - X)RT$$
$$P_{H_2O} = CO_0(\theta - X)RT$$
$$P_{H_2} = P_{CO_2} = CO_0(X)RT$$

where θ is the molar ratio of steam to CO in the inlet stream. The first associative mechanism proposed, LH1, did not fit the data generated for several of the experimental conditions and was therefore eliminated (FIT = 1.49).

LH2 has ten parameters to be optimized while the redox mechanism has four, and the ROM has five. Data for every experimental condition was fit for each kinetic model to determine the respective kinetic parameters, and the results are shown in Table 4. For each model, the activation energy decreased as catalyst weight was increased. The estimated apparent activation energy for the LH2, ROM, and redox models ranged from 62-66 kJ/mol, 29-45 kJ/mol, and 75-77 kJ/mol, respectively, depending on the WHSV. The ROM showed the largest decrease in the apparent activation energy of the three models. As WHSV decreased, the apparent activation energy reached a plateau at a greater catalyst weight than that of WHSV #2. The apparent activation energy estimated by the ROM fell within the range of previous kinetic studies over a Cu-based catalyst but was still lower than other reported values[11, 12]. For the ROM, the reaction order with respect to carbon monoxide and steam was shown to be the most sensitive to experimental conditions fluctuating between 0.48-1.27 and 0.37-1.22 respectively, whereas the reaction orders for the carbon dioxide and hydrogen remained relatively constant. The Langmuir Hinshelwood model predicted apparent activation energies that were more consistent in magnitude than the ROM and the apparent activation energy of 65 kJ/mol is well within typical reporting ranges over a $CuO/ZnO/Al_2O_3$ catalyst[11]. The activation energies reported are apparent activation energies. The values for the activation energy reported between different mechanistics will not necessarily be comparable. The ROM is a simple kinetic model that does not account for any mechanistic aspects and the models are fitting different numbers of parameters.

Table 3. Rate law expressions for each kinetic model tested.

Kinetic Model	Rate Equation
Langmuir-Hinshelwood 2	$-r_{CO} = \frac{k\left(P_{CO}P_{H_2O} - \frac{P_{CO_2}P_{H_2}}{K_e}\right)}{\left(1 + K_{CO}P_{CO} + K_{H_2O}P_{H_2O} + K_{H_2}{}^{0.5}P_{H_2}{}^{0.5} + K_{CO_2}P_{CO_2}P_{H_2}{}^{0.5}\right)^2}$
Redox	$-r_{CO} = \frac{k\left(P_{H_2O} - \frac{P_{CO_2}P_{H_2}}{P_{CO}K_e}\right)}{1 + \frac{K_{CO}P_{CO_2}}{P_{CO}}}$

ROM	$-r_{CO} = kP_{CO}^{a}P_{H_2O}^{b}P_{H_2}^{c}P_{CO_2}^{d}(1-\beta)$

Model discrimination

The mean absolute error (MAE), root mean squared error (RMSE), and goodness of fit (FIT) analyses were used to compare how well each model fit the experimental data. Further discrimination of the models was accomplished using the Akaike information criterion (AIC). This allowed for comparison between models with a different number of parameters. The results of each statistical test are shown in Table 5. For all of the statistical tests, lower values indicate a better fit. Upon comparison of the three statistical tests, the three models give similar values. However, the LH2 model provided the best overall fit to the experimental data for each WHSV and 200-400 °C.

Table 4. Estimated parameters for the proposed kinetic models at WHSV #2 at temperatures from 200-400 °C

Parameter	LH2*	Redox*	ROM
$\ln(k_0)$	16.98±0.21	16.94±1.20	4.21±1.07)
E_a	64.93±3.84	77.2±14.89	32.97±7.8
ln(Kco)	-1.48±1.03	-	-
ΔHco	21.93±7.08	-	-
$\ln(K_{H2O})$	-5.56±3.77	-	-
ΔH_{H2O}	15.12±4.2	-	-
$\ln(K_{H2})$	-3.82±1.16	-	-
ΔH_{H2}	12.05±6.56	-	-
$\ln(K_{CO2})$	-1.72±0.70	-3.09±2.16	-
ΔH_{CO2}	32.85±7.89	-35.61±9.31	-
a	-	-	0.95±0.44
b	-	-	0.73±0.46
c	-	-	-0.77±0.21
d	-	-	-0.59±0.14

* ± indicates standard deviation

The ROM and the redox model produced similar test values for each set of conditions, but the ROM appeared to show a more predictive trend when plotted alongside the experimental data. Therefore, the ROM was the second best fit to the experimental data over all conditions.

Associative mechanisms, as well as a ROM, have been shown to provide the best fits in several previous works[11, 12, 37]. The good fit of the associative mechanism makes sense when compared to literature because Cu-based catalysts are typically regarded as low-temperature shift catalysts and the experimental temperature range overlaps with that of the LTS. Both the Langmuir-Hinshelwood and ROM are statistically good fits that can be used for different purposes in future work regarding the intermediate-temperature shift (ITS). For a purely kinetic simulation, the Langmuir-Hinshelwood kinetics would be the most accurate mechanistic representation of the experimental data. These mechanistic models have utility for designing new processes that require a high degree of accuracy over a wide range of conditions. However, for numerical models of more advanced systems that are computationally intensive, such as a computational fluid dynamics model for bio-oil hydropyrolysis where the WGS is a secondary process, the ROM could be used to reduce the overall computation cost while maintaining accuracy. This is especially true if these numerical models do not require mechanistic level details in the implementation of reaction schemes. Even though the ROM can reduce computational resources, that should not stop efforts to identify good mechanistic models. ROMs are only applicable for the specific experimental conditions for which they were derived, and the simplicity will sacrifice accuracy. All in all, each type of model has their own advantages and disadvantages depending on the application.

Table 5. Goodness of fit results for kinetic models over each WHSV.

WHSV	LH#2			Redox			ROM		
	1	2	3	1	2	3	1	2	3
RMSE	0.045	0.048	0.034	0.059	0.060	0.071	0.064	0.056	0.074
MAE	0.038	0.040	0.030	0.050	0.049	0.058	0.053	0.045	0.052
FIT	0.004	0.003	0.001	0.007	0.005	0.007	0.010	0.004	0.007
AIC	-273.7	-270.5	-274.1	-261.5	-252.4	-254.4	-276.5	-231.1	-222.8

Conclusions

The kinetics of the water-gas shift reaction over a Cu-based catalyst at intermediate-temperature shift (ITS) conditions (200-400 °C) are reported in this study. At ITS conditions, kinetics data were obtained for three space velocities and were fit to two associative Langmuir-Hinshelwood mechanistic models (LH1 and LH2) as well as a ROM and redox model. The associative LH2 best fit the experimental data on the basis of the statistical analysis of the regression based on the goodness of fit tests and Akaike Information Criterion (AIC). The LH2 model yielded apparent activation energy between 60-80 kJ/mol over varying WHSVs whereas the ROM yielded apparent activation energies from 29-47 kJ/mol. The reaction order for CO_2 and H_2 remained constant over all WHSVs while the exponents for CO and H_2O fluctuated from between 0.48-1.27 and 0.37-1.22, respectively. Both the mechanistic and empirical kinetic models have potential for application concerning the WGS. The Langmuir-Hinshelwood model would yield the most accurate results based on the kinetic experiments, whereas the ROM can be used for incorporation into models that are computationally expensive to reduce computational power while retaining accuracy.

Conflicts of Interest

There are no conflicts of interest to declare.

Acknowledgments

The authors would like to acknowledge funding support for this research by the U.S. Department of Agriculture (USDA) Agriculture and Food Research Initiative, grant number 2015-6021-24121.

Notes and references

1. D. S. Newsome, *Catalysis Reviews Science and Engineering*, 1980, **21**, 275-318.
2. P. Moriarty and D. Honnery, *International Journal of Hydrogen Energy*, 2009, **34**, 31-39.
3. T. L. Marker, L. G. Felix, M. B. Linck and M. J. Roberts, *Environ. Prog. Sustainable Energy*, 2012, **31**, 191-199.
4. A. Campen, K. Mondal and T. Wiltowski, *International Journal of Hydrogen Energy*, 2008, **33**, 332-339.
5. O. D. Mante, F. A. Agblevor, S. T. Oyama and R. McClung, *Bioresource Technology*, 2012, **111**, 482-490.
6. R. Y. Chein, Y. H. Lin, Y. C. Chen, Y. P. Chyou and J. N. Chung, *International Journal of Hydrogen Energy*, 2014, **39**, 18854-18862.
7. C. Rhodes, B. Peter Williams, F. King and G. J. Hutchings, *Catal. Commun.*, 2002, **3**, 381-384.
8. T. L. LeValley, A. R. Richard and M. Fan, *International Journal of Hydrogen Energy*, 2014, **39**, 16983-17000.
9. D. C. Grenoble, M. M. Estadt and D. F. Ollis, *Journal of Catalysis*, 1981, **67**, 90-102.
10. W. F. Podolski and Y. G. Kim, *Industrial & Engineering Chemistry Process Design and Development*, 1974, **13**, 415-421.
11. J. L. Ayastuy, M. A. Gutiérrez-Ortiz, J. A. González-Marcos, A. Aranzabal and J. R. González-Velasco, *Industrial & Engineering Chemistry Research*, 2005, **44**, 41-50.
12. D. Mendes, V. Chibante, A. Mendes and L. M. Madeira, *Industrial & Engineering Chemistry Research*, 2010, **49**, 11269-11279.
13. M. Zhu and I. E. Wachs, *ACS Catalysis*, 2016, **6**, 722-732.
14. R. J. B. Smith, M. Loganathan and S. Shantha Murthy, *Journal*, 2010, **8**.
15. C. Rhodes, G. J. Hutchings and A. M. Ward, *Catalysis Today*, 1995, **23**, 43-58.
16. C. Ratnasamy and J. P. Wagner, *Catalysis Reviews*, 2009, **51**, 325-440.
17. J. E. Kubsh and J. A. Dumesic, *AIChE Journal*, 1982, **28**, 793-800.
18. P. Kumar, E. Akpan, H. Ibrahim, A. Aboudheir and R. Idem, *Industrial & Engineering Chemistry Research*, 2008, **47**, 4086-4097.
19. R. L. Keiski, T. Salmi, P. Niemistö, J. Ainassaari and V. J. Pohjola, *Applied Catalysis A: General*, 1996, **137**, 349-370.
20. P. M. Mortensen, J. D. Grunwaldt, P. A. Jensen, K. G. Knudsen and A. D. Jensen, *Applied Catalysis A: General*, 2011, **407**, 1-19.
21. A. R. K. Gollakota, M. Reddy, M. D. Subramanyam and N. Kishore, *Renewable and Sustainable Energy Reviews*, 2016, **58**, 1543-1568.
22. S.-I. Fujita, M. Usui and N. Takezawa, *Journal of Catalysis*, 1992, **134**, 220-225.
23. T. Salmi and R. Hakkarainen, *Applied Catalysis*, 1989, **49**, 285-306.
24. S. Li, Y. Lu, L. Guo and X. Zhang, *International Journal of Hydrogen Energy*, 2011, **36**, 14391-14400.
25. S. Bhatia, J. Beltramini and D. D. Do, *Catalysis Today*, 1990, **7**, 309-438.
26. T. Umegaki, Y. Kojima and K. Omata, *Materials*, 2015, **8**, 5414.
27. C.-H. Zhang, Y. Yang, B.-T. Teng, T.-Z. Li, H.-Y. Zheng, H.-W. Xiang and Y.-W. Li, *Journal of Catalysis*, 2006, **237**, 405-415.
28. M. Wojdyr, *Journal of Applied Crystallography*, 2010, **43**, 1126-1128.
29. H. S. Fogler, *Essentials of Chemical Reaction Engineering*, Prentice Hall, 2011.
30. J. J. Carberry, in *Catalysis: Science and Technology*, eds. J. R. Anderson and M. Boudart, Springer Berlin Heidelberg, Berlin, Heidelberg, 1987, DOI: 10.1007/978-3-642-93278-6_3, pp. 131-171.
31. U. Hanefeld and L. Lefferts, *Catalysis: An Integrated Textbook for Students*, Wiley, 2017.
32. V. Prasad, A. M. Karim, A. Arya and D. G. Vlachos, *Industrial & Engineering Chemistry Research*, 2009, **48**, 5255-5265.
33. H. S. Fogler, *Elements of Chemical Reaction Engineering*, Prentice Hall PTR, 2006.
34. P. Smirniotis and K. Gunugunuri, *Water Gas Shift*

Reaction: Research Developments and Applications, Elsevier Science, 2015.

35. E. Armstrong and T. Hilditch, *Proceedings of the Royal Society of London. Series A, Containing Papers of a Mathematical and Physical Character (1905-1934)*, 1920, **97**, 265-273.
36. D. Mohammady Maklavany, A. Shariati, B. Roozbehani and M. R. Khosravi Nikou, *American Journal of Oil and Chemical Technologies*, 2016, **4**.
37. Y. Choi and H. G. Stenger, *Journal of Power Sources*, 2003, **124**, 432-439.
38. N. V. Kulkova and M. I. J. Temkin, *Zh. Fiz. Khim.*, 1949, **23**, 695-713.
39. T. Salmi, L. E. Lindfors and S. Boström, *Chemical Engineering Science*, 1986, **41**, 929-936.
40. Y. Lei, N. W. Cant and D. L. Trimm, *Chemical Engineering Journal*, 2005, **114**, 81-85.
41. F. Gökaliler, Z. I. Önsan and A. E. Aksoylu, *Catalysis Communications*, 2013, **39**, 70-73.
42. P. Castaño, J. M. Arandes, B. Pawelec, J. L. G. Fierro, A. Gutiérrez and J. Bilbao, *Industrial & Engineering Chemistry Research*, 2007, **46**, 7417-7425.
43. O. Oyedeji, C. S. Daw, N. Labbe, P. Ayers and N. Abdoulmoumine, *Bioresource Technology*, 2017, **244**, 525-533.
44. E. Granada, P. Eguía, J. A. Comesaña, D. Patiño, J. Porteiro and J. L. Miguez, *Journal of Thermal Analysis and Calorimetry*, 2013, **113**, 569-578.
45. F. N. Fritsch and R. E. Carlson, *SIAM Journal on Numerical Analysis*, 1980, **17**, 238-246.
46. H. Akaike, *IEEE Transactions on Automatic Control*, 1974, **19**, 716-723.
47. N. A. Koryabkina, A. A. Phatak, W. F. Ruettinger, R. J. Farrauto and F. H. Ribeiro, *Journal of Catalysis*, 2003, **217**, 233-239.
48. C. V. Ovesen, B. S. Clausen, B. S. Hammershøi, G. Steffensen, T. Askgaard, I. Chorkendorff, J. K. Nørskov, P. B. Rasmussen, P. Stoltze and P. Taylor, *Journal of Catalysis*, 1996, **158**, 170-180.
49. H. Yahiro, K. Murawaki, K. Saiki, T. Yamamoto and H. Yamaura, *Catalysis Today*, 2007, **126**, 436-440.
50. D.-W. Jeong, W.-J. Jang, J.-O. Shim, W.-B. Han, H.-S. Roh, U. H. Jung and W. L. Yoon, *Renewable Energy*, 2014, **65**, 102-107.
51. M. J. L. Ginés, N. Amadeo, M. Laborde and C. R. Apesteguía, *Applied Catalysis A: General*, 1995, **131**, 283-296.
52. J.-P. Shen and C. Song, *Catalysis Today*, 2002, **77**, 89-98.
53. G. Yuan and M. A. Keane, *Chemical Engineering Science*, 2003, **58**, 257-267.
54. J. Pérez-Ramírez, R. J. Berger, G. Mul, F. Kapteijn and J. A. Moulijn, *Catalysis Today*, 2000, **60**, 93-109.
55. P. Kumar and R. Idem, *Energy & Fuels*, 2007, **21**, 522-529.
56. M. J. L. Ginés, A. J. Marchi and C. R. Apesteguía, *Applied Catalysis A: General*, 1997, **154**, 155-171.